Electron Deformation Density for the "Supershort" Cr—Cr Bond: A Joint Experimental and Theoretical Study

André Mitschler,[1a] Bernard Rees,*[1a,c] Roland Wiest,[1b] and Marc Benard[1b]

Contribution from ER 139 du CNRS and Université Louis Pasteur, 67070 Strasbourg Cédex, France. *Received May 18, 1982*

Abstract: The charge density distribution in "supershort" metal–metal quadruple bonds has been investigated both experimentally in tetrakis(μ-2-hydroxy-6-methylpyridine)dichromium [$Cr_2(mhp)_4$] and theoretically in tetrakis(μ-dimethylphosphoniumylidenedimethylido)dichromium. The two compounds have similar molecular structures and practically identical Cr–Cr bond lengths (1.879 and 1.885 Å, respectively). Three low-temperature (74 K) X-ray data sets were collected on $Cr_2(mhp)_4$: one high-order set was used to determine the atomic positional and thermal parameters, and two sets with a maximum resolution $2(\sin\theta)/\lambda$ of 1.52 Å^{-1} were used to compute the charge density. A systematic bias having been detected (and later on corrected) in one of those, the effect of systematic error on the final deformation density maps is discussed. The quantum-chemical LCAO calculations were performed ab initio with configuration interaction. The experimental and theoretical deformation density maps are qualitatively very similar. The most striking feature is a strong charge density accumulation between the Cr atoms, with a maximum at the bond midpoint and an extension over the π and δ regions. The peak height (experimental, 0.4; theoretical, 0.3 e Å^{-3}) is comparable to deformation density peaks between first-row atoms. A comparison is performed with experimental and theoretical density distributions previously obtained for dichromium and dimolybdenum tetracarboxylates. An analysis of the computed maps leads to the definition of a "quadruple-bond pattern" remaining qualitatively similar over a very large range of metal–metal distances.

Introduction

In recent years a large number of quadruply bonded Cr–Cr compounds have been synthesized. This class of compounds presents some rather puzzling characteristics, in particular, the large range of the metal–metal bond lengths, which varies over as much as 0.7 Å.[2] Such large differences indicate that behind the formal concept of quadruple bonding the real bonding situations may be quite different. Theoretical investigations on dichromium tetraformate[3] have shown that neither the "pure quadruple bond" $\sigma^2\pi^4\delta^2$ nor the nonbonding configuration $\sigma^2\delta^2\delta^{*2}\sigma^{*2}$, which both arise from SCF-level calculations, correspond to a realistic description of the system. Strong correlation effects require an elaborate configuration interaction (CI) treatment, which does confirm the quadruply bonding configuration as the leading term but reduces drastically the formal bond order.

The importance of the presence or absence of axial ligands is not yet completely clear. From ab initio calculations[3] on anhydrous and dihydrated chromium formate, it was concluded that the axially situated water molecules had no major influence on the strength of the Cr–Cr bond. A more accurate configuration interaction expansion performed in the meantime[4] did not modify this conclusion. However, an impressive correlation has been established experimentally between the strength of the chromium–(axial ligand) interaction and the length of the Cr–Cr bond.[5] In particular, among the more recently discovered compounds are those with a so-called "supershort" bond, none of which has axial ligands, the axial access to the metal being generally impeded by bulky side groups. In these compounds the bonding configuration is likely to be closer to $\sigma^2\pi^4\delta^2$.

Dihydrated chromium acetate has already been submitted to an experimental low-temperature charge density analysis.[6] A similar study at room temperature was made on molybdenum acetate.[7] Molybdenum quadruply bonded compounds behave less erratically than the chromium analogues; for example, the range of the Mo–Mo bond length is much narrower. An ab initio SCF calculation[7] showed that $\sigma^2\pi^4\delta^2$ is the ground state, and a limited CI calculation gave a weight of 66% to the leading term $\sigma^2\pi^4\delta^2$, while for chromium formate[3] it was only 18%.[8] This difference in bonding corresponds to differences in the charge density distribution, as established by the two experimental determinations. In both cases the density is near zero on the metal–metal bond axis, but a torus of positive residual density is seen around this axis in the molybdenum compound while in the chromium compound a very shallow and slightly positive residue is spread out over a large region.

We report here the results of a low-temperature determination of charge distribution by X-ray diffraction ("X-X" method) in a compound with a supershort Cr–Cr bond: tetrakis(μ-2-hydroxy-6-methylpyridine)dichromium, or $Cr_2(mhp)_4$. The structure of this compound, crystallized with one molecule of CH_2Cl_2, has been determined by X-ray diffraction by Cotton et al.[9]

So that a better understanding of the metal–metal bonding mechanism in this class of compounds might be gained, the wave function of another complex of chromium displaying a "supershort" quadruple bond, tetrakis(μ-dimethylphosphoniumylidenemethylido)dichromium, $[(CH_3)_2P(CH_2)_2]_4Cr_2$, was calculated at a configuration interaction level. The ligand $(CH_3)_2P(CH_2)_2$, modelized into $H_2P(CH_2)_2$, was chosen for its simplicity (the calculation of $Cr_2(mhp)_4$ at the same level of accuracy would be prohibitive). Although the ligands $H_2P(CH_2)_2$ and mhp are different, we believe that this does not affect appreciably the Cr–Cr bonding, as is attested by the similarity of the bond lengths, which differ only by 0.006 Å.

Experimental Section

Crystallized $Cr_2(mhp)_4 \cdot CH_2Cl_2$ was kindly supplied by Professor F. A. Cotton. By recrystallization in chlorobenzene under argon, it was possible to grow crystals of $Cr_2(mhp)_4$ free of solvent molecules, as was confirmed by a room-temperature X-ray structure determination. This

(1) (a) Laboratoire de Cristallochimie, ERA 08 du CNRS. (b) Laboratoire de Chimie Quantique, ER 139 du CNRS. (c) To whom correspondence should be addressed at the Laboratoire de Cristallographie Biologique, Institut de Biologie Moléculaire et Cellulaire, 67084 Strasbourg Cédex, France.
(2) Cotton, F. A. *Acc. Chem. Res.* **1978**, *11*, 225–232.
(3) Bénard, M. *J. Am. Chem. Soc.* **1978**, *100*, 2354–2362.
(4) Wiest, R.; Bénard, M., unpublished results.
(5) Cotton, F. A.; Ilsley, W. H.; Kaim, W. *J. Am. Chem. Soc.* **1980**, *102*, 3464–3474.
(6) Bénard, M.; Coppens, P.; De Lucia, M. L.; Stevens, E. D. *Inorg. Chem.* **1980**, *19*, 1924–1930.
(7) Hino, K.; Saito, Y.; Bénard, M. *Acta Crystallogr., Sect. B* **1981**, *B37*, 2164–2170.
(8) For the chromium formate, a much more accurate CI treatment, involving all configurations generated from the set of eight Cr–Cr bonding and antibonding orbitals, yielded for the $\sigma^2\pi^4\delta^2$ leading configuration a weight of only 9%.[4] A still smaller weight was obtained by Atha et al.[22]
(9) Cotton, F. A.; Fanwick, P. E.; Niswander, R. H.; Sekutowski, J. C. *J. Am. Chem. Soc.* **1978**, *100*, 4725–4732.

0002-7863/82/1504-7501$01.25/0

Table I. Crystallographic Data

	room temp	74 K
space group $P\bar{1}$, $Z = 2$		
a/Å	13.637	13.459 (2)
b/Å	10.570	10.537 (2)
c/Å	8.748	8.693 (1)
α/deg	78.22	78.36 (2)
β/deg	102.26	102.01 (2)
γ/deg	94.24	94.34 (2)
V/Å^3	1205.6	1180.2 (5)
D_{calcd}/(g/cm^3)	1.478	1.509

Table II. X-ray Diffraction Measurements

	data set		
	1	2	3
X radiation	Mo Kα	Mo Kα	Mo Kα
(sin θ)/λ range/Å^{-1}	<0.76	<0.76	0.76–1.19
no. of measmts	8702	13458	5786
rescan condition	none	$\sigma_{count}^2(I)/I > 10$	none
no. of indep reflctns	8471	8506	5239
% of reflctns measd	99	99	51, 65 < 2θ < 77°
			25, 77 < 2θ < 92°
			10, 92 < 2θ < 115°

determination (Philips PW1100 diffractometer, Cu Kα radiation) yielded results in agreement with those of Cotton et al.[9] but will not be discussed here.

The low-temperature measurements were performed on a Picker FACS-1 diffractometer, with Mo Kα radiation and a graphite monochromator. A recorded temperature of 74 ± 0.5 K was maintained by circulation of liquid nitrogen through a beryllium cryostat (Cryogenic Associates, locally modified). This temperature is a little below the nitrogen boiling point at normal pressure because of the depression caused by pumping at the outlet of the transfer line.

The crystal had been shaped into a sphere of 0.21 ± 0.01 mm diameter. Absorption of X rays by the crystal is very small (μ = 9.38 cm^{-1}, μR = 0.099, transmission coefficient between 0.863 and 0.865); the diffracted intensities were nevertheless corrected for it, as well as for absorption by the cryostat walls, as these corrections are routinely incorporated in our data processing procedure.

The space group is $P\bar{1}$ with two molecules per unit cell. The cell parameters, measured at 74 K and at room temperature, are reported in Table I.

Two complete low-resolution data sets and one high-resolution data set were measured. Relevant data are given in Table II. In the case of the high-resolution data set, only the reflections expected to be sufficiently strong were measured. For this purpose, the structure factors F_c were calculated on the basis of the crystal structure established from the low-resolution data. The reflections for which $E_c = F_c/(\sum f_j^2)^{1/2}$ was larger than a given threshold were stored in the memory of the PDP 8A computer, which monitors the diffraction measurements.

All measurements were done by the step-scan method. The step was 0.05° in 2θ, and the measuring time was 2 s/step.

About 1600 reflections were also measured without a monochromator but with Zr-filtered Mo Kα radiation. Those reflections had a much lower (by a factor of about 5) peak/background ratio and were used only to check the effect of the monochromator on the other data sets. It was found that the scale of data set 1 was dependent on the diffractometer χ angle, which is indicative of a slight miscentering of the crystal. The data were corrected (largest corrections: ±3% of the observed intensities) and their esd's raised accordingly.

Data Processing. Since the measurements had taken a very long time, systematic changes in the scale factor, as monitored by the periodic measurement of three standard reflections, could not be avoided. Rescaling was done with the local program STANDARD, which also adds to the counting variance a term considering discrepancies between the standard reflections.

Data sets 1 and 2 were first processed separately and finally combined with appropriate weights. The agreement factor between the two sets of intensities, $\sum^1/_2(|I_1 - \bar{I}| + |I_2 - \bar{I}|)/\sum\bar{I}$, was 0.033.

Positional and Thermal Parameters. The positional and thermal parameters used in the calculation of the deformation density were obtained by least-squares refinement from the high-angle data set, except for the hydrogen atoms. Atomic coordinates and anisotropic temperature factors are deposited as supplementary material. Some relevant figures of merit

Table III. Least-Squares Refinements

	data set	
	1 + 2	3
rejectn criterion	none	$F^2 < 2\sigma(F^2)$
no. of reflctns considered (N)	8515	5239
no. of parameters (p)	403	307
$R(F) = \Sigma \lvert F_o - F_c \rvert / \Sigma \lvert F_o \rvert$	0.050	0.057
$R_w(F^2) = [\Sigma w(F_o^2 - F_c^2)^2 / \Sigma w F_o^4]^{1/2}$	0.093	0.102
$S = [\Sigma w(F_o^2 - F_c^2)^2/(N-p)]^{1/2}$	2.11	1.03
scale factor	2.407 (1)	2.381 (2)

Table IV. Nonrigid Motion of Hydrogen Atoms (Mean Square Amplitudes)

	ring hydrogens		methyl hydrogens	
	this work	neutron values[a]	this work	neutron values[b]
C–H elongation/Å^2	0.027 (4)	0.004	0.015 (4)	0.004
in-plane bending/deg^2	−76 (10)	26	−33 (10)	42
out-of-plane bending (or methyl torsion)/deg^2	0 (13)	54	50 (30)	225
			160 (40)	
			60 (30)	
			100 (30)	

[a] In $C_6H_6Cr(CO)_3$ at 78 K.[11] [b] In acetamide at 23 K.[10]

are given in Table III. Since there were too many parameters to be refined together in a complete-matrix refinement, each refinement cycle was split into two: in the first part the parameters of the inner part of the molecule were refined and in the second those of the outer part, atoms of the intermediate region being common to both refinements. A tentative refinement of an extinction parameter showed that extinction was negligible.

The hydrogen atoms are a special problem when no neutron data are available. Their parameters were first determined by least-squares refinement from the averaged low-angle data set. This procedure resulted as usual in an underestimation of the CH bond lengths. We chose to keep the refined bond direction but to rescale the bond lengths to more correct values: 1.079 Å for the methyl hydrogens, as observed by neutron diffraction in acetamide at 23 K,[10] and 1.087 Å for the ring hydrogens, as in $C_6H_6Cr(CO)_3$ at 78 K.[11]

A correct determination of the temperature parameters is more difficult. The anisotropic mean square amplitudes of the hydrogen atoms were written as U(rigid body) + ΔU. The U(rigid body) tensors were obtained in a thermal motion analysis[12] performed on each of the four wings of the molecule, not including either Cr or H atoms (see below). Each ΔU depends on three parameters: the CH elongation amplitude and the C–C–H in-plane and out-of-plane bending amplitudes. Furthermore the same value may be assumed for each of these three parameters for all ring hydrogens on one hand and all methyl hydrogens on the other, except for the methyl C–C–H out-of-plane bending (which is undistinguishable from the methyl rotation amplitude). This may depend on steric effects and therefore be different for each methyl group. There are thus 9 parameters to determine for the 24 hydrogen atoms. This was done by least-squares refinement, directly on the X-ray square structure factors, in a modification of the refinement program LINEX.

The results are quoted in Table IV and compared to the neutron values for the two compounds mentioned above.[10,11] The stretching amplitudes are seen to be consistently larger and the bending amplitudes smaller than the neutron values. This may be due to the shape of the hydrogen charge distribution, more expanded in the C–H direction and more contracted in the perpendicular plane than the spherically averaged bonded hydrogen atom[13] used in the least-squares refinement. Except for the methyl torsion the values retained finally were the neutron values of Table IV. The squared amplitudes of methyl torsion were taken from the X-ray refinement but increased by (70 deg^2) to correct for the probable bias mentioned. It is interesting to note that, even with this correction, the amplitude of methyl rotation is generally smaller than in acetamide even

(10) Jeffrey, G. A.; Ruble, J. R.; McMullan, R. K.; De Frees, D. J.; Binkley, J. S.; Pople, J. A. *Acta Crystallogr., Sect. B* **1980**, *B36*, 2292–2299.
(11) Rees, B.; Coppens, P. *Acta Crystallogr., Sect. B* **1973**, *B29*, 2516–2528.
(12) Schomaker, V.; Trueblood, K. N. *Acta Crystallogr., Sect. B* **1968**, *B24*, 63–76.
(13) Stewart, R. F.; Davidson, E. R.; Simpson, W. T. *J. Chem. Phys.* **1965**, *42*, 3175–3187.

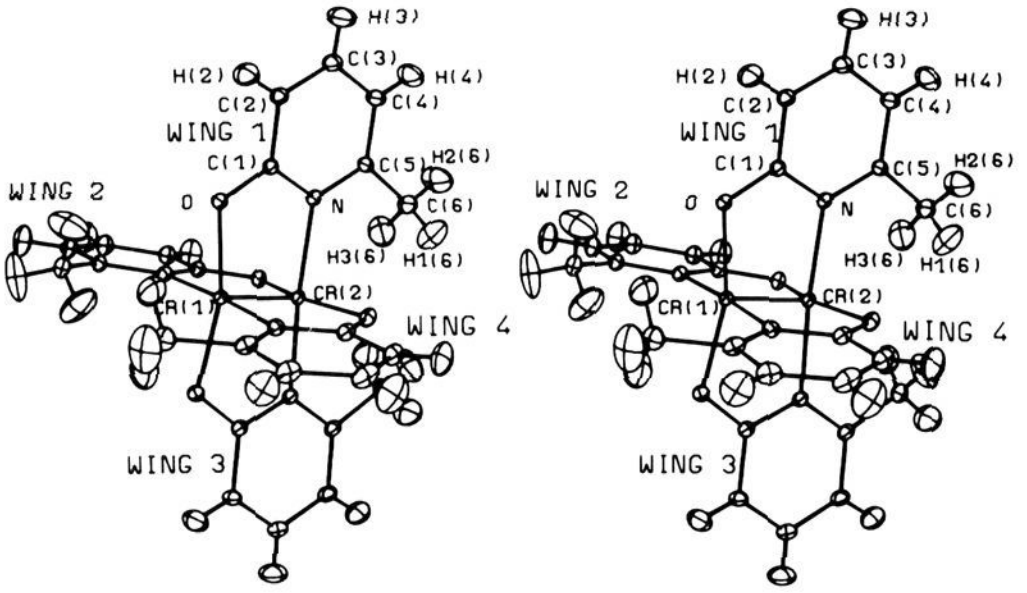

Figure 1. Molecule of $Cr_2(mhp)_4$ in the crystal at 74 K. The probability of presence at a given time inside the equiprobability ellipsoids is 50%.

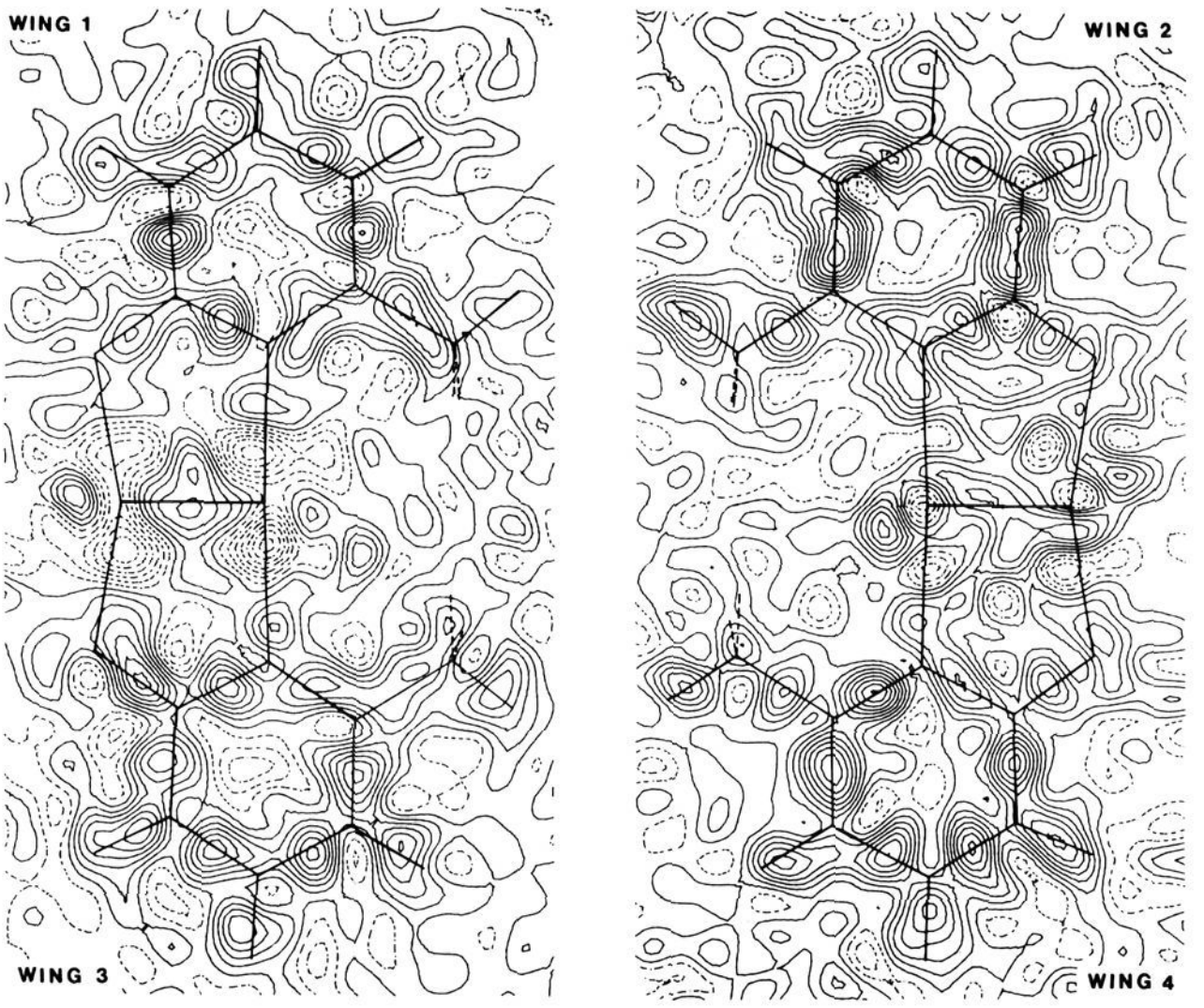

Figure 2. Experimental deformation density in the planes of the four molecular wings. Each plane is defined by the nuclei of Cr(1), Cr(2), and C(3). The spacing of the equidensity contours is 0.10 e $Å^{-3}$. Negative contours are dashed lines; zero and positive contours solid lines.

though the temperature is 50 K higher, probably because of a stronger steric hindrance.

Deformation Density. The deformation density was defined as usual, as the difference between the total electron density and the free spherical atom model, with positional and thermal parameters determined as above. Maps were computed separately from data sets 1 and 2 and then from the combined set. The deformation density was finally averaged with the assumption that, in spite of the distortions observed in the crystal, molecular charge density was still of D_{2d} symmetry as in the ideal molecule, at least not too far from the Cr–Cr axis. Nonaveraged maps (from the combined data set) are shown in Figure 2 and averaged maps in Figures 3 and 6.

Random and Systematic Errors. The deformation density maps first calculated from the two separate data sets looked quite similar, except in the chromium region. Each chromium atom was surrounded by two peaks, in a symmetric disposition and in the same direction in a given map. But the direction was different for each data set and not in accordance with the symmetry of the molecule. These peaks were particularly large with the first data set, where, as mentioned above, we detected a systematic dependence of the observed intensity on the diffractometer χ angle. The effect of such systematic error on the deformation density may be rationalized as follows. The observed structure factors may be considered as the product of the true structure factors by an error function depending on the position in reciprocal space. The observed electron density is then the convolution of the correct density by the Fourier transform of this error function. The error function being real (it affects the magnitude of the structure factors, not their phase), its Fourier transform is centrosymmetric. The result is that spurious peaks (or depressions) will show up, symmetrically disposed, and always in the same direction, around each atomic position. With the assumption that the parameters of the calculated density are not affected by an error of the same kind, the height of such a peak will be proportional to that of the total density peak of the atom, hence it will be observed essentially around the heaviest atoms. Although these spurious features have no a priori reason to conform to the molecular symmetry, there is obviously a danger in many cases to misinterpret them as true electron density features, because of the symmetry and regularity of their disposition.

In the case of our first data set, an error function of χ only is symmetric around the crystal rotation axis and so will be its Fourier transform: indeed the peaks observed were close to the direction of the rotation axis.

Fortunately, such systematic errors are essentially canceled by the averaging procedure assuming noncrystallographic symmetry, because they do not conform to the molecular symmetry. The only exception is

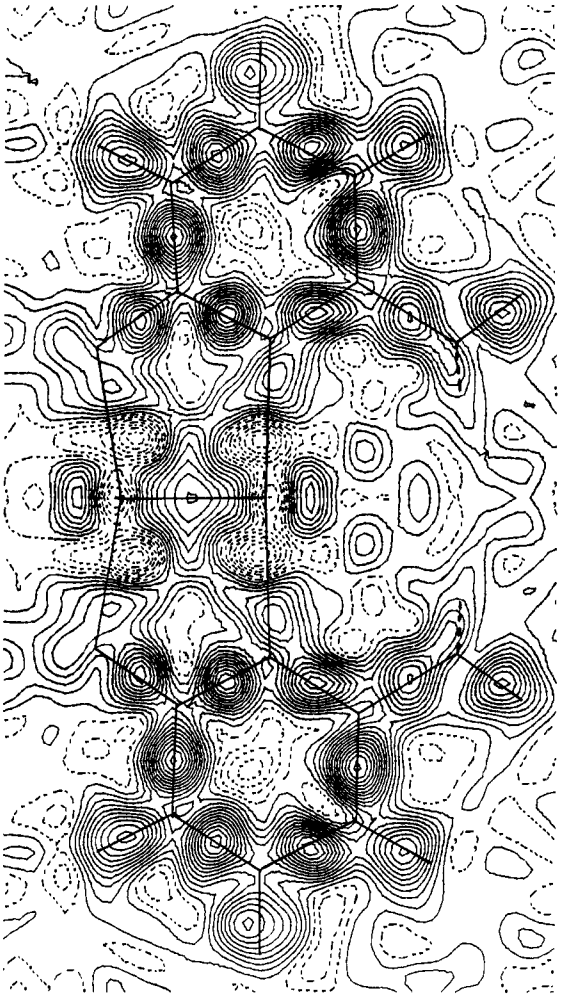

Figure 3. Average experimental deformation density in the plane of a wing (spacing of contours 0.05 e Å^{-3}).

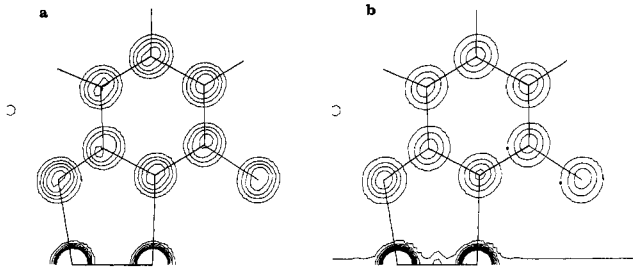

Figure 4. Estimated standard deviations of the experimental deformation density: (a) in the plane of one wing; (b) of the average deformation density (spacing of contours 0.025 e Å^3). Outside the atomic regions, and far from the Cr–Cr axis in (b), the esd is equal to 0.082 e Å^{-3} in (a) and 0.041 e Å^{-3} in (b). At the chromium positions the esd culminates at 0.6 e Å^{-3} (not all contours are shown). The esd of the error due to the spherical model used in the calculation of the scale factor was assumed to be 0.5% of the total density.

the direction of the Cr–Cr bond, which is therefore unreliable in the vicinity of each metal nucleus. In all other regions the errors may be assumed to be essentially random. Maps of the esd of the deformation density are shown in Figure 4, before and after averaging.[14] Clearly, in the second case the correlation between errors at averaged points needs to be considered.

Molecular Orbital Calculations

The theoretical density maps were obtained from ab initio LCAO–MO–SCF + CI calculations on $[H_2P(CH_2)_2]_4Cr_2$ carried out with the ASTERIX system of programs.[15] The Gaussian basis

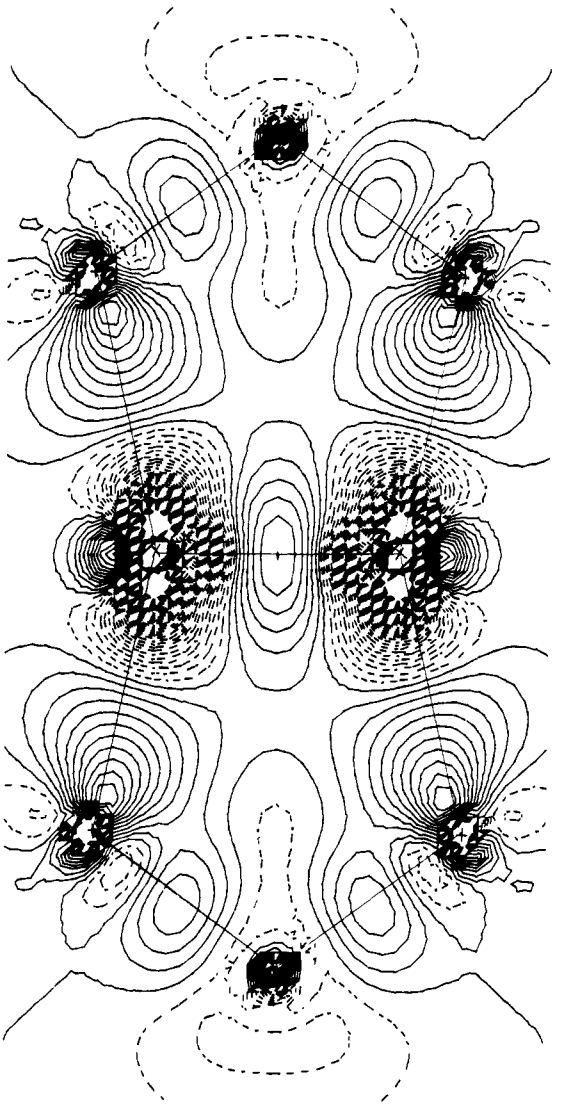

Figure 5. Theoretical deformation density in the plane of a wing (spacing of contours 0.05 e Å^{-3}).

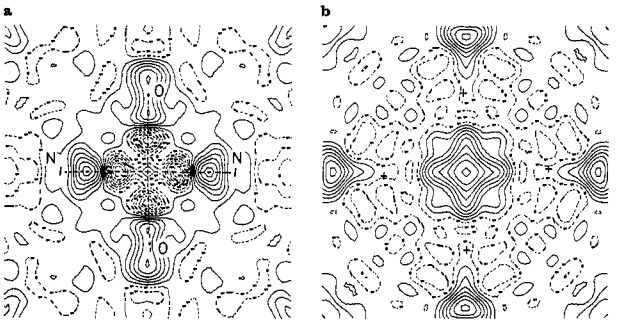

Figure 6. Average experimental deformation density in planes perpendicular to the Cr–Cr axis: (a) plane through the metal nucleus; (b) plane through the midpoint of the bond (spacing of contours 0.05 e Å^{-3}).

set used for Cr was taken from the (13,7,5) set of Hyla-Kryspin et al.[16] and incremented with one p function of exponent 0.15 and one diffuse d function of exponent 0.08. It was contracted to [5,3,3], that is, minimal for internal and 4p shells, double-ζ for 4 s shells, and triple-ζ for 3d shells. Basis sets (11,7), (9,5), and

(14) Rees, B. *Acta Crystallogr., Sect. A.* **1978**, *A34*, 254–256.

(15) Bénard, M.; Dedieu, A.; Demuynck, J.; Rohmer, M. M.; Strich, A.; Veillard, A.; Wiest, R. "ASTERIX: A System of Programs for the UNIVAC 1110" (unpublished). Bénard, M.; Barry, M. *Comput. Chem.* **1979**, *3*, 121–124.

(16) Hyla-Kryspin, I.; Demuynck, J.; Strich, A.; Bénard, M. *J. Chem. Phys.* **1981**, *75*, 3954–3961.

Table V. Molecular Geometry

	wing 1	wing 2	wing 3	wing 4	indiv std dev	mean	rms dev from mean[a]
			Bond Lengths/Å[f]				
Cr-O	1.974	1.967	1.968	1.970	0.002	1.970	0.003
Cr-N	2.061	2.075	2.063	2.075	0.002	2.068	0.008
N-C(1)	1.358	1.358	1.353	1.362	0.003	1.358	0.004
C(1)-C(2)	1.422	1.418	1.430	1.410	0.004	1.420	0.008
C(2)-C(3)	1.377	1.374	1.385	1.378	0.004	1.378	0.005
C(3)-C(4)	1.406	1.407	1.398	1.409	0.004	1.405	0.005
C(4)-C(5)	1.388	1.382	1.389	1.377	0.004	1.384	0.006
C(5)-N	1.357	1.361	1.362	1.361	0.003	1.360	0.002
C(5)-C(6)	1.499	1.510	1.500	1.513	0.003	1.506	0.007
C(1)-O(1)	1.294	1.306	1.296	1.301	0.003	1.299	0.005
			Valence Angles/deg				
Cr-Cr-O	99.16	99.63	99.41	99.80	0.06	99.50	0.28
Cr-Cr-N	92.02	91.70	91.79	91.64	0.06	91.75	0.18
Cr-O-C(1)	115.6	115.7	115.2	115.3	0.2	115.5	0.2
Cr-N-C(1)	115.4	115.4	115.3	115.1	0.2	115.3	0.1
N-C(1)-C(2)	119.8	120.6	120.6	120.1	0.2	120.3	0.4
C(1)-C(2)-C(3)	118.7	119.4	117.9	119.2	0.3	118.8	0.7
C(2)-C(3)-C(4)	120.7	119.6	120.6	120.1	0.3	120.3	0.5
C(3)-C(4)-C(5)	118.5	118.9	119.5	118.6	0.3	118.9	0.5
C(4)-C(5)-N	121.0	121.9	120.4	121.6	0.3	121.2	0.7
C(5)-N-C(1)	121.3	119.7	121.1	120.3	0.2	120.6	0.7
O-C(1)-N	117.8	117.5	117.9	118.0	0.2	117.8	0.2
C(6)-C(5)-N	115.8	116.0	116.5	116.5	0.2	116.2	0.4
			Dihedral Angles/deg[g]				
XCr(1)Cr(2), X'Cr(1)Cr(2)[b] (X and X' bonded to Cr(1))	90.72	91.30	87.31	90.67	0.08	90	1.82
Cr(1)Cr(2)X, Cr(1)Cr(2)X'[b] (X and X' bonded to Cr(2))	91.73	90.71	89.16	88.40	0.09	90	1.50
XCr(1)Cr(2)X'	+1.11	+2.12	+1.53	+3.38	0.09	+2.04	0.99
			Refined Hydrogen Positions[d]				
			H of Pyridine Ring				
C-H(cor)/Å	0.96 (2)	0.99 (3)	0.96 (2)	0.96 (6)	0.02	0.97	0.01
dist to pyridine plane	−0.01 (3)	0.02 (3)	−0.04 (1)	0.01 (3)	0.02	−0.01	0.03
			Methyl H				
C-H(cor)/Å	0.99 (1)	1.00 (1)	0.97 (3)	0.97 (3)	0.02	0.98	0.01
C-C-H/deg	111 (3)	109 (1)	111 (2)	110 (1)	1	110	1
Me torsion angle[e]/deg	14 (2)	−21 (2)	2 (2)	−5 (2)	1	−3	15
			Pyridine Planes (C_5N Ring)				
planarity criterion S[c]	2.13	1.22	2.82	4.10			
d[Cr(1)]/Å	−0.0811	0.0038	−0.1241	0.0995	0.0004	−0.0255	0.0988
d[Cr(2)]/Å	−0.1245	−0.0819	−0.1414	0.2473	0.0004	−0.0251	0.1833
dihedral angles[b]	93.2	83.5	79.4	89.2	0.6	96.3	6.1

[a] $\Sigma (d_i - \bar{d})^2/(n-1)$. [b] Between wing i and wing $i+1$. [c] $S = [1/(n-3)\Sigma d_i^2/\sigma^2(d_i)]^{1/2}$, where d_i is the distance to the plane and $n = 6$. For a planar ring, S should be close to 1 and $(n-3)S^2$ distributed as a χ^2 variable with $n-3$ degrees of freedom. [d] The values quoted are the mean values between the three homologous hydrogen atoms together with the rms deviation (in brackets, on the last digit). [e] Zero if one hydrogen is in the C(4)C(5)C(6) plane, eclipsed with C(4). [f] Corrected for thermal motion; Cr-Cr = 1.8794 (6) Å. [g] X and X' are N or O.

(4), respectively,[17] were used for phosphorus, carbon, and hydrogen and contracted to split valence, that is, [4,3], [3,2], and [2].

The interatomic distances were taken from the experimental determination of Cotton et al.[18] However, the angles of the ligand were slightly modelized in order to increase the symmetry of the system from C_{4h} to D_{4h}. The carbons of the dimethylido group were assumed to be tetrahedral. Indeed, a significant deviation from tetrahedral character would lead to unrealistic hindrance between hydrogen atoms belonging to neighboring CH_2 fragments.

The SCF closed-shell calculation performed on the quadruply bonding configuration $\sigma^2\pi^4\delta^2$ yielded an energy of −3759.4124 au. The CI expansion included the configurations generated from all possible excitations arising inside the set of metal–metal bonding and antibonding orbitals.[19] Since both the π_x and π_y bonding orbitals are almost equally distributed between two occupied MO's in the SCF wave function, we were compelled to increase from 8 to 10 the size of the orbital set active in the CI process. This active set generated 1820 configurations in the A_{1g} representation, yielding for the ground state an energy lowering of 0.3989 au.

Table VI. Dominant Configurations in the CI Calculation of $[H_2P(CH_2)_2]Cr_2$[a]

excitations	weight	excitations	weight
leading confign ($\sigma^2\pi^4\delta^2$)	0.551	$\bar{\pi}^2 \rightarrow \bar{\pi}^{*2}$	0.021
$\delta^2 \rightarrow \delta^{*2}$	0.193	$\pi^2\delta^2 \rightarrow \pi^{*2}\delta^{*2}$	0.013
$\pi\delta \rightarrow \pi^*\delta^*$	0.036	$\bar{\pi}^2\delta^2 \rightarrow \bar{\pi}^{*2}\delta^{*2}$	0.013
$\bar{\pi}\delta \rightarrow \bar{\pi}^*\delta^*$	0.036	$\pi\bar{\pi} \rightarrow \pi^*\bar{\pi}^*$	0.019
$\pi^2 \rightarrow \pi^{*2}$	0.021	$\pi\bar{\pi}\delta^2 \rightarrow \pi^*\bar{\pi}^*\delta^{*2}$	0.013

[a] The contributions of the two MO's with strong metal $d_{xz}(\pi)$ weight have been added together, as for the $d_{yz}(\bar{\pi})$ contributions.

(17) Huzinaga, S. *J. Chem. Phys.* **1965**, *42*, 1293–1302.
(18) Cotton, F. A.; Hanson, B. E.; Ilsley, W. H.; Rice, G. W. *Inorg. Chem.* **1979**, *18*, 2713–2717.
(19) The four-index integral transformation and the configuration interaction expansion were performed with a system of programs written by M.B. and R.W. The CI program is based on the algebraic formulation of the Unitary Group Approach.[20]
(20) See, for instance: Hinze, J., Ed. "The Unitary Group for the Evaluation of Electronic Energy Matrix Elements"; Springer-Verlag: West Berlin, 1981.

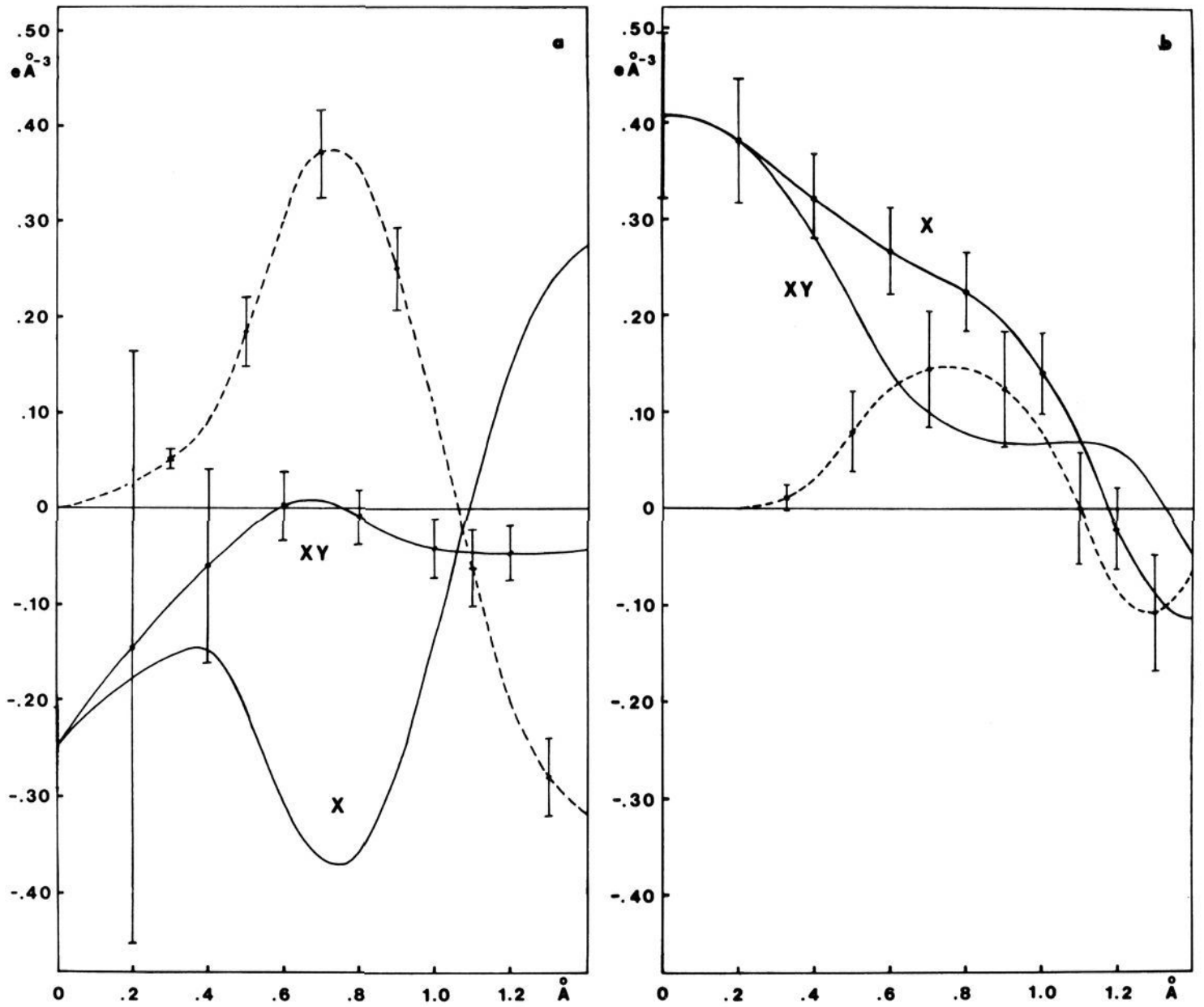

Figure 7. Average experimental deformation density in the planes of Figure 6. The curves represent the density in the diagonal direction xy, in ligand direction x (averaged), and their difference (dashed curve), vs. r, the distance from the bond axis, (a) at the Cr nucleus and (b) at the bond midpoint. The error bars represent $\pm\sigma$ intervals. For the sake of clarity the error intervals of the deformation density are shown only in one direction, since they are practically the same in the other direction at the same r. Error estimates of the difference take into account the correlation between the substracted densities.[14]

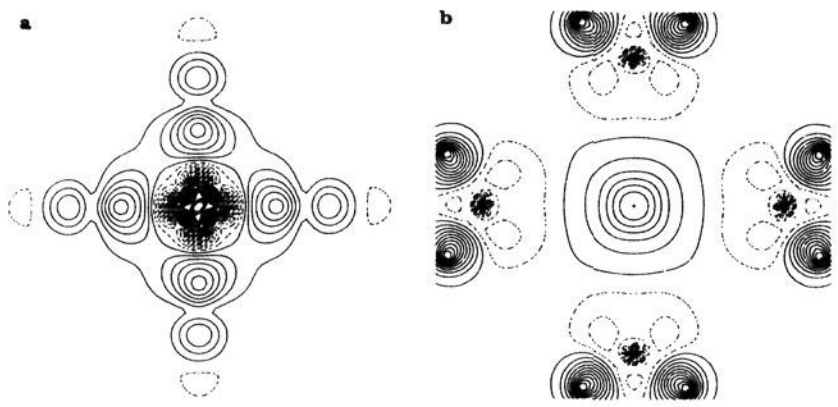

Figure 8. Theoretical deformation density in planes perpendicular to the Cr–Cr axis: (a) plane through the metal nucleus; (b) plane through the midpoint of the bond (spacing of contours 0.05 e Å^{-3}).

The weight of the $\sigma^2\pi^4\delta^2$ is then 55%.[21] In the CI expansion, eight dominant configurations including the leading term are found associated with a CI coefficient larger than 0.1, and 23 other important configurations are over the threshold of 0.05. The weights of the dominant configurations, labeled in terms of metal–metal bonding → antibonding excitations, are listed in Table VI.

Figures 5 and 8 show the deformation density in three different planes of $[H_2P(CH_2)_2]_4Cr_2$. The deformation density is defined as the difference between the total density computed from the CI wave function and the spherically averaged ground-state atoms. The SCF wave functions of the free atoms were computed in the same basis as the molecule.

(21) A CI expansion performed on the same set of 10 active orbitals but limited to configurations generated from single and double excitations only (85 configurations) yielded an energy lowering of 0.2941 au and a weight of 70% for the leading term. These results confirm that the usual limitation to single and double excitations is not sufficient to obtain a correct description of the quadruple Cr–Cr bond, even at such a short distance.[3]

Table VII. Natural-Orbital Analysis of the CI Wave Functions for $[H_2P(CH_2)_2]Cr_2$, $Cr_2(O_2CH)_4$, and $Mo_2(O_2CH)_4$

	natural-orbital population					
	σ	π	δ	δ^*	π^*	σ^*
$[H_2P(CH_2)_2]Cr_2$ (this work)	1.92	3.59	1.39	0.61	0.41	0.08
$Cr_2(O_2CH)_4$ (d_{Cr-Cr} = 2.20 Å)[22]	1.62	2.69	1.14	0.85	1.30	0.38
$Mo_2(O_2CH)_4$ (d_{Mo-Mo} = 2.09 Å)[22]	1.89	3.69	1.65	0.35	0.31	0.11

Interpretation of the CI Results. A comparison can be made with the recent ab initio CI calculations performed by Atha, Hillier, and Guest[22] on $Mo_2(O_2CH)_4$ and $Cr_2(O_2CH)_4$, assuming for this last system Cr–Cr bond lengths of 2.20 and 2.36 Å. In this study, the description of the left–right correlation effects is performed at a similar level of accuracy as in the present work, and additional configurations were added to account for a part of the radial and angular correlation effects.[22] Such a comparison obviously shows that $[H_2P(CH_2)_2]Cr_2$, $Mo(O_2CH)_4$, and $Cr_2(O_2CH)_4$ belong to the same class of binuclear complexes in which the metal–metal covalent interactions involve to a certain extent the σ, π, and δ bonding orbitals. The differences between these three systems are related to large changes in strength occurring in the four components of the metal–metal bond. These bond

(22) Atha, P. M.; Hillier, I. H.; Guest, M. F. *Mol. Phys.* **1982**, *46*, 437–448.

strengths are immediately visualized from the relative weight of the metal–metal bonding and antibonding orbitals obtained from the natural-orbital analysis. This analysis, given in Table VII for the three systems, shows that, in the frame of the covalent metal–metal quadruple bond, the supershort Cr–Cr system is different from both $Mo_2(O_2CH)_4$ and $Cr_2(O_2CH)_4$. In dichromium tetraformate, all four components of the metal–metal bond are contaminated to a large extent by the antibonding orbitals, thus drastically reducing the formal bond order from 4 to 1.5.[22] In $Mo_2(O_2CH)_4$, the correlation energy is reduced by a factor of 3 with respect to $Cr_2(O_2CH)_4$ and the decrease of orbital mixing affects in a similar way the four components of the Mo–Mo bond.[22] The formal bond order given by the natural-orbital analysis is 3.2[22] (Table VII), which can be considered as rather close to a pure quadruple-bond model.[3]

In $Cr_2[H_2P(CH_2)_2]_4$, the "supershort" Cr–Cr system investigated in the present work, the formal bond order is 2.9 (Table VII), significantly lower than for $Mo_2(O_2CH)_4$, in spite of the much shorter metal–metal distance (1.89 Å for Cr–Cr instead of 2.09 Å for Mo–Mo). As for $Mo_2(O_2CH)_4$ the σ and π components of the Cr–Cr coupling remain strongly bonding with relatively small contamination from the corresponding antibonding orbitals (Table VII). On the contrary, there is a substantial mixing of the δ and δ^* orbitals accounting for most of the bond order decrease. Considering the δ interaction alone, the supershort Cr–Cr system behaves very much like the dichromium tetracarboxylates, for which this component appears almost elusive (Table VII). However, this rather weak δ bond can still be detected from the "squared" shape of the central electron accumulation disk, as obtained from the theoretical deformation density distribution reported in the present work.

Even though X-ray diffraction experiments and the CI wave function analysis are in agreement concerning the existence of some remaining δ interaction in supershort systems, it appears that this δ component is consistently very weak in the quadruple chromium—chromium bond. If this conclusion were to be general for $Cr\overset{4}{-}Cr$, it might appear in contradiction with the prominent role devoted to the δ bond which is preventing rotation around the metal–metal axis from the eclipsed to the staggered position.[23] However, it is worth noting that in all known systems with a quadruple Cr–Cr bond any deviation from the eclipsed conformation is prevented by the cage structure of the ligands.[24] No $Cr\overset{4}{-}Cr$ system with a nonrigid structure is known, and more specifically, no $M_2X_8^{4-}$ ion (X = Cl, Br) has been characterized with chromium, even though such systems have been considered with other metals as precursors to the synthesis of most quadruply bonded complexes.

Discussion

Molecular Geometry and Thermal Motion. The molecule $Cr_2(mhp)_4$ is shown in Figure 1. Like chromium acetate, it has four chemically equivalent wings around the Cr–Cr axis, but the ideal symmetry of the molecule is only D_{2d} instead of D_{4h} because, in contrast to the acetate ligand, methylpyridine cannot have any symmetry element other than its own plane.

The essential characteristics of the molecular geometry as observed in the crystal are reported in Table V. The chromium–chromium bond length is found slightly shorter than in the room-temperature study of Cotton et al.:[9] 1.879 (1) instead of 1.889 (1) Å. A similar gap between Cr–Cr distances obtained at low temperature and at room temperature was found for $Cr_2(O_2CCH_3)_4 \cdot 2H_2O$.[6] These relatively large contractions of the Cr–Cr bond lengths can be explained from the shallowness of the Cr–Cr potential curve predicted by theoretical calculations.[3,4] All other values are given in Table V for each wing together with the mean and the "internal" (column 6) and "external" (i.e., from the dispersion around the mean, column 8) esd's. Comparison of the two estimates shows whether or not the observed distortions are significant.

Table VIII. Rigid-Body Thermal Motion of the Methylpyridinone Ligands (without Hydrogen Atoms)[a]

translation tensor	wing 1	wing 2	wing 3	wing 4
T_x	98	84	94	100
T_y	92	112	110	132
T_z	102	77	102	91
rotation tensor	**wing 1**	**wing 2**	**wing 3**	**wing 4**
L_x	2.0	2.3	2.0	3.0
L_y	4.3	4.3	3.6	3.3
L_z	6.6	3.6	5.9	8.2

[a] x is normal to the ligand plane, and z is along the metal–metal bond axis. Values for the translation tensor are in 10^{-4} Å^2, and values for the rotation tensor are in deg^2.

The result is that there are little distortions of bond lengths and valences angles, even when Cr–O or Cr–N bonds are implied—although somewhat more in that case than inside the mhp ligands. There is however some flexibility in the position of the ligands, as shown by the spread of the dihedral angles between the pyridine planes and by the distances to those planes of the chromium atoms. Interestingly, the dihedral angles between XCrCr planes (X = O or N) are much closer to 90°. The XCrCrX′ dihedral angles, with X and X′ in eclipsed positions, are all of the same sign, which shows that the whole molecule is slightly twisted, with a torsion angle of about 2°. The largest XCrCrX′ dihedral angle also corresponds to the less planar pyridine ring.

The pyridine bond lengths are quite in agreement with the values observed by Cotton et al.[9] But the differences between the C–C bond lengths here become significant, since the esd's are smaller than at room temperature. The alternating of shorter and longer C–C bonds is in perfect accordance with the postulated equilibrium between two tautomeric forms, one aromatic, the other with localized bonds.[9,25]

Considering the methyl groups, one of the C–H bonds always eclipses, or nearly eclipses, the ring C–C bond. This conformation may optimize the van der Waals interactions of the two other hydrogen atoms with the methyl group of the opposite ring, even though the energies involved are quite small considering the rather large H···H distances (2.78 Å average).

The shortest van der Waals contacts between neighboring molecules involve hydrogen atoms. The shortest O···H distance is 2.37 Å, the shortest C···H 2.52 Å, and the shortest H···H 2.27 Å (six other H···H distances are less than 2.40 Å). Those values are somewhat shorter than the sum of van der Waals radii, presumably because of the unit cell contraction at low temperature. The external atoms closest to chromium are also hydrogens, however, at a distance of at least 3.79 Å from Cr(1) and 3.96 Å from Cr(2). This shows how efficient is the protection of the metal atoms by the methyl groups against the approach of any possible axial ligand.

A rigid-body thermal motion analysis[12] has shown that the contribution of the internal modes of the four ligand wings to the amplitude of motion of the atoms C, N, and O is negligible: in each case the rms value of $\mathbf{U} - \mathbf{U}$(rigid body) is of the order of $\sigma(\mathbf{U})$. (0.0004–0.0008 Å^2 for the former quantity, compared to 0.0005–0.0009 Å^2 for the latter). On the other hand, the Cr–ligand bonding frame is not completely rigid, as expected. Squared amplitudes of rigid-body translation and rotation of the four ligand wings are given in Table VIII. It is seen that while translational motions are roughly isotropic, rotation occurs preferentially around the Cr–Cr axis.

As a result of this analysis, the C–C, C–N, and C–O bond lengths reported in Table V have been corrected with the assumption of a rigid motion of the corresponding ligand wing; the Cr–O, Cr–N, and also ring C–H bond lengths were corrected for

(23) Cotton, F. A. *Chem. Soc. Rev.* **1975**, *4*, 27–53.

(24) The ion $Cr_2(CH_3)_8^{4-}$ could appear as an exception, but the Li^+ counterions, each facing four (CH_3) ligands might prevent any flexibility of the system. See: Krausse, J.; Marx, G.; Schödl, G. *J. Organomet. Chem.* **1970**, *21*, 159–168.

(25) Penfold, B. R. *Acta Crystallogr.* **1953**, *6*, 591–600.

a riding motion of the second atom on the first. Methyl C–H bonds were corrected for methyl torsion. These corrections were however quite small and always less than the esd of the bond length, except for some C–H bonds (largest correction 0.035 Å).

The rigid-bond test[26] gave the following results for the rms difference in **U** of bonded atoms in the direction of the bond: 0.0012 Å^2 for C–C, C–O, and C–N bonds (expected from the esd's 0.0010 Å^2), 0.0017 Å^2 for Cr–O and Cr–N bonds (expected 0.0006 Å^2). This again indicates the relative flexibility of the Cr–ligand bonding, contrasting with the rigidity of the mhp ligands.

Charge Density Distribution. Before discussing and comparing the theoretical and the experimental deformation densities, it must be remembered that no quantitative comparison can be made between the two series of maps, not only because the ligands are different but also because the experimental density is affected by thermal motion and by the limited resolution of the measurements. With this restriction in mind, the experimental maps displayed in Figures 3 and 6 show however an obvious and striking similarity with the corresponding theoretical maps of Figures 5 and 8, respectively, as far as the Cr–Cr bond region is concerned.

The comparison of the observed and computed density distributions along the Cr–Cr axis leads to the following remarks. In both distributions, the midpoint of the bond corresponds to a peak of density. An agreement on this point appears important, since it was not obtained for other systems displaying a quadruple bond, namely, $Cr_2(O_2CH)_4$[6] and $Mo_2(O_2CH)_4$.[7] For these two systems, theoretical distributions also displayed a peak at the center of symmetry, even though this maximum was extremely soft for the chromium acetate.[6] On the contrary, experimental distributions figured the center of symmetry as a saddle point lying between two diffuse accumulation zones located in the π and possibly δ bonding regions.[6,7] The origin of this saddle point has never been clearly rationalized, since this feature appears in contradiction with the σ overlap bringing the largest contribution to the metal–metal bond.[27] The changes occurring in the theoretical density map when going from the chromium acetate (d_{Cr-Cr} = 2.36 Å) to the "supershort" Cr–Cr bond and more specifically the rise of the central peak from 0.1 to 0.3 e Å^{-3} simply suggest a progressive increase of the overall bond strength in correlation with the decrease of the bond length.

The experimental density at the midpoint of the Cr–Cr bond is 0.41 e Å^{-3}, which is, to our knowledge, the largest value ever observed for a metal–metal bond. Several considerations strengthen our confidence in the validity of this experimental result: (a) essentially the same density was obtained in a separate treatment of the two X-ray data sets; (b) the bond midpoint is sufficiently distant from the Cr nuclei to be outside the zone of largest possible systematic error; (c) at positions symmetric to the bond midpoint relative to the Cr nuclei the deformation density is close to zero, while, as shown above, peaks due to systematic errors are symmetric about the Cr nuclei. The theoretical deformation density culminates at 0.30 e Å^{-3}. This is slightly less than the experimental value, whereas one would expect the opposite because of the effect of thermal motion and limited resolution. However, this effect is probably not very large in this region, where no steep variations of density occur.

The central accumulation zone extends over the whole σ, π, and δ bonding region. In the theoretical deformation density (Figure 8b), this accumulation is shaped as a narrow disk roughly squared in the xy directions.[33] It is worth noting that this topography remains quite similar in the three theoretical distributions computed up to now for systems with a quadruple metal–metal bond. The main difference comes from the peak heights, which are 0.1 e Å^{-3} for $Cr_2(O_2CH)_4$, 0.15 e Å^{-3} for $Mo_2(O_2CH)_4$, and 0.3 e Å^{-3} for $Cr_2[H_2P(CH_2)_2]_4$. This confirms the existence of a permanent "quadruple-bond pattern" either weak or strong according to the considered system but remaining qualitatively similar over a surprisingly wide range of metal–metal distances.

The experimental evidence for a disk of electron accumulation extending over the σ, π, and δ bonding region is in complete agreement with the covalent nature of the chromium–chromium interaction. However, the alternative assumption of a weak antiferromagnetic coupling between two high-spin chromium atoms recently suggested by Corrêa de Mello et al.[34] is not expected to account for a significant electron buildup along the metal–metal axis. This has been shown in the case of $Cr_2(O_2CH)_4$,[6] for which the deformation density has been computed from a UHF broken symmetry wave function similar to the one advocated by Corrêa de Mello (Figures 7c and 8c of ref 6). Contrary to the CI expansion also reported in ref 6, the UHF wave function did not yield any electron accumulation in the whole region of metal–metal interaction. It therefore appears that the hypothesis of an antiferromagnetic coupling is unlikely to be realistic, at least in the range of the Cr–Cr "supershort" bond.

In the experimental map (Figure 6b), the deformation of the accumulation disk along the xy directions is only observed at distances larger than 1 Å from the bond axis. Closer to the axis, the situation seems reversed, with a density larger in the x or y than in the xy direction. An explanation of such features would not be straightforward. However, the difference of density in the two directions is at most about twice its esd (see Figure 7) and thus not quite significant.

As already mentioned about the theoretical density distributions of $Cr_2(O_2CH)_4$ and $Mo_2(O_2CH)_4$,[6,7] the configuration interaction treatment does not modify the pattern of the computed deformation density, even though the total energy and the wave function are drastically modified. However, the relatively small refinements induced by CI on deformation density are mainly responsible for the differences between the distributions computed for $Cr_2(O_2CH)_4$ and $Cr_2[H_2P(CH_2)_2]_4$. At the SCF level, the peak height obtained for $Cr_2(O_2CH)_4$ was 0.21 e Å^{-3}. Configuration interaction reduced this peak to 0.10 e Å^{-3} in accord with a relatively high population of the σ^* orbital. For $Cr_2[H_2P(CH_2)_2]_4$, the peak height is decreased from 0.33 to 0.30 e Å^{-3} only with a population of 0.08 e for the σ^* orbital. In other respects, the central accumulation disk computed for $Cr_2[H_2P(CH_2)_2]_4$ is less "squared" in the xy directions at the CI than at the SCF level, thus illustrating the important rise of the δ^* population (0.61 e) brought in by CI.

Considering the density around chromium, positive residues are seen on the bond axis, outside the molecule, with their symmetric counterparts merging into the metal–metal bond density. This is the less reliable region of the experimental deformation density, since, as discussed above, it may be affected by systematic error effects which cannot vanish upon averaging. However, the theoretical maps show similar residues, only sharper and closer to the metal center, as expected from the infinite resolution and the

(26) Hirshfeld, F. L. *Acta Crystallogr., Sect. A* **1976**, *A32*, 239–244.

(27) The σ bond has been assumed to be the strongest among the four σ, π, and δ metal–metal bonds since the early scheme of Cotton[28] showing the σ–σ^* separation bigger than the π–π^*, bigger itself than δ–δ^*. This has been corroborated later by photoelectron spectroscopy[29] and by several theoretical studies, either SCF–Xα[30] or ab initio accounting for correlation effects,[22,31] including the present work. The origin of the saddle point observed in the experimental deformation density maps of $Cr_2(O_2CCH_3)_4 \cdot 2H_2O$ and $Mo_2(O_2CCH_3)_4$ had been tentatively traced to the possible influence of axial ligands on the Cr–Cr σ bond.[6] However, this explanation does not hold for the molybdenum tetraacetate, which does not exhibit significant interactions in axial positions (Mo···O = 2.645 Å).[32]

(28) Cotton, F. A. *Inorg. Chem.* **1965**, *4*, 334–336.

(29) Coleman, A. W.; Green, J. C.; Hayes, A. J.; Seddon, E. A. *J. Chem. Soc. Dalton Trans.* **1979**, 1057–1064. Berry, M.; Garner, C. D.; Hillier, I. H.; Mcdowell, A. A.; Walton, I. B. *Chem. Phys. Lett.* **1980**, *70*, 350–352 and references therein.

(30) Norman, J. G., Jr.; Kolari, H. J. *J. Chem. Soc., Chem. Commun.* **1975**, 649–651. Norman, J. G., Jr.; Kolari, H. J.; Gray, H. B.; Trogler, W. C. *Inorg. Chem.* **1977**, *16*, 987–993. Cotton, F. A.; Kalbacher, B. J. *Ibid.* **1977**, *16*, 2386–2396 and references therein. Norman, J. G., Jr.; Ryan, P. B. *J. Comput. Chem.* **1980**, *1*, 59–63.

(31) Bénard, M.; Veillard, A. *Nouv. J. Chim.* **1977**, *1*, 97–99. Guest, M. F.; Hillier, I. H.; Garner, C. D. *Chem. Phys. Lett.* **1977**, *48*, 587–589. Hay, P. J. *J. Am. Chem. Soc.* **1978**, *100*, 2897–2898.

(32) Cotton, F. A.; Mester, Z. C.; Webb, T. R. *Acta Crystallogr., Sect. B* **1974**, *B30*, 2768–2770. Cotton, F. A.; Extine, M.; Gage, L. D. *Inorg. Chem.* **1978**, *17*, 172–176.

(33) In the molecular frame z is along the Cr–Cr axis, and x is in a ligand plane. xy designates a diagonal direction.

(34) Corrêa de Mello, P.; Edwards, W. D.; Zerner, M. C. *J. Am. Chem. Soc.* **1982**, *104*, 1440–1442.

absence of thermal motion. Similar features had been observed in molybdenum acetate,[7] but not in chromium acetate,[6] in accordance with MO calculations.

This accumulation is difficult to interpret, since it apparently does not involve the d orbitals of chromium. The d_{z^2} orbital population, computed from the CI wave function, is 1.003 e. This is practically identical with the average d-orbital population in the promolecule, which is 1 e. Moreover, on the theoretical map, the peak is located at only 0.34 Å from the nucleus. At such a short distance, an effect due to a small contraction of the 3s and/or 3p shells cannot be excluded. It is interesting to notice that these external peaks have been observed only for systems that are insensitive to axial coordination.[7]

The most significant feature of the experimental deformation density in the metal region (Figure 6a) is the lack of density in the direction of the ligands. There is no significant difference between the Cr–N and Cr–O directions within about 1 Å from Cr, and the two directions have thus been averaged for the calculation of the curves of Figure 7a. The figure shows that the difference is very large compared to its esd and points thus to a much lower occupancy of $3d_{x^2-y^2}$ than of $3d_{xy}$. Its low occupancy enables $d_{x^2-y^2}$ to work as an acceptor orbital for the oxygen and nitrogen lone pairs in dative σ bonds.

This character is common to all systems displaying a quadruple metal–metal bond. However, the population of the $d_{x^2-y^2}$ orbital is markedly higher for $Cr_2[H_2P(CH_2)_2]_4$ than for $Cr_2(O_2CH)_4$ and $Mo_2(O_2CH)_4$. From less than 0.25 e for the tetraformates, the computed $d_{x^2-y^2}$ population jumps to 0.57 e for $Cr_2[H_2P(CH_2)_2]_4$. This is probably specific to the $H_2P(CH_2)_2$ ligand, since the carbon lone pair is much higher in energy than the oxygen lone pair and therefore induces a stronger interaction with the empty $d_{x^2-y^2}$ metal orbital.

A character that is more specific to the "supershort" Cr–Cr bond is the existence of a ligand–metal–metal angle significantly bigger than 90° (about 104° for $Cr_2[H_2P(CH_2)_2]_4$[18]). This angle induces some interaction between the ligand lone pairs and the π^* orbitals of the metal, which might contribute to the slight increase observed in the overall π population (2.19 e for $Cr_2[H_2P(CH_2)_2]_4$ instead of 2.02 e for $Cr_2(O_2CH)_4$).[35]

Another feature is directly visible on both experimental and theoretical maps (Figures 6a and 8a) in agreement with the results of the population analysis: this is the relatively low population of the d_{xy} orbitals. This population is only 0.88 e for $Cr_2[H_2P(CH_2)_2]_4$ instead of 1.07 e for $Cr_2(O_2CH)_4$ and 1.05 e for $Mo_2(O_2CH)_4$. The density maps derived in the plane that is perpendicular to the metal–metal axis and contains one metal atom (Figure 8a) can be compared with similar maps derived for $Mo_2(O_2CH)_4$[7] in order to visualize the relative lack of d_{xy} population. Both experimental and theoretical maps derived for $Mo_2(O_2CH)_4$ display significant density accumulation in the xy direction. In contrast with this pattern, the corresponding map observed for $Cr_2mhp)_4$ is just "less negative" in the xy than in the $x^2 - y^2$ direction. The theoretical map obtained for $Cr_2[H_2P(CH_2)_2]_4$ appears quite consistent with experiment.[36] It appears difficult to decide whether this lack of d_{xy} population might correspond to some electron migration toward the δ bonding region. The assignment by a Mulliken population analysis of electrons located in this area might indeed become hazardous.[35] The "squared" shape of the central accumulation disk (Figure 8b) denotes an appreciable remainder of δ bonding, in spite of the high weight of the δ^* orbital in the CI expansion. However, similar evidence for δ bonding was found from the density distribution of $Mo_2(O_2CH)_4$ without any depopulation of the d_{xy} orbitals.

Acknowledgment. We are indebted to Professor F. A. Cotton for sending us samples of the compound. We also wish to thank Professor C. Burgraff for his inestimable assistance in running the low-temperature experiments. Quantum-chemical calculations have been performed at the Centre de Calcul du CNRS at Strasbourg-Cronenbourg. We thank the staff for their cooperation.

Registry No. $Cr_2(MPh)_4$, 67634-82-6; $[(CH_3)_2P(CH_2)_2]_4Cr_2$, 68525-29-1; Cr, 7440-47-3.

Supplementary Material Available: Listings of observed and calculated structure factors and of the positional and thermal parameters for $Cr_2(mhp)_4$ (20 pages). Ordering information is given on any current masthead page.

(35) However, the presence of a diffuse d orbital in the basis set of chromium makes less reliable the space partitioning associated with the Mulliken population analysis. Small changes in the *d*-orbital population must therefore be analyzed with caution.

(36) Four small peaks can be characterized in the xy direction at 0.33 Å from the Cr nuclei (Figure 8a). These small and sharp peaks are expected to vanish in a "X-X" distribution, because of thermal motion and limited resolution. That was not the case for the relatively extended accumulations obtained for $Mo_2(O_2CH)_4$.[7]

Pentacyanoferrate(II) Complexes of Amino Acids

Henrique E. Toma,*[1a] Alzir A. Batista,[1b] and Harry B. Gray*[1c]

Contribution from the Instituto de Quimica, Universidade de São Paulo, CEP 0.1000, São Paulo, Brazil, and No. 6605 from the Arthur Amos Noyes Laboratory, California Institute of Technology, Pasadena, California 91125. *Received February 22, 1982*

Abstract: The electronic spectra and the kinetic and thermodynamic properties of an extensive series of (amino acid)-pentacyanoferrate(II) complexes have been investigated in aqueous solution. The spectra of the complexes containing aminocarboxylate ligands are similar to that of $Fe(CN)_5NH_3^{3-}$, with Dq estimated to be ~0.233 μm^{-1}. For the methionine, histidine, and methionine sulfoxide complexes, Dq values are 0.239, 0.248, and 0.286 μm^{-1}, respectively. The rates of formation of the complexes are 240–370 M^{-1} s^{-1} for zwitterionic amino acids and 18–30 M^{-1} s^{-1} for mononegatively charged and 9 M^{-1} s^{-1} for dinegatively charged α-aminocarboxylate ligands (25 °C and μ = 0.10 M). The specific rates increase as the number of C–C bonds separating the coordination site from the carboxylate group is increased. The kinetic and thermodynamic properties (dissociation rate, stability constant, reduction potential) of each (amino acid)pentacyanoferrate depend strongly on the donor/acceptor nature of its amino acid ligating group. The imidazole group of histidine is unique in the sense that it stabilizes both iron(II) and iron(III) states (K_{II} = 5.9 × 10^5; K_{III} = 1.1 × 10^6 M^{-1}).

Amino acids occupy a special place in the coordination chemistry of transition-metal ions.[2-5] Although many complexes of amino acids are described in the literature, most of them are chelate species involving α-aminocarboxylate binding. Not enough

0002-7863/82/1504-7509$01.25/0